Joint Special Interest Group meeting between euspen and ASPE
Advancing Precision in Additive Manufacturing
KU Leuven, Belgium, September 2023
www.euspen.eu

Manufacturing constraints for Cu paste based 3D micro-extrusion

Samanwitha Kolli[1,2], Marleen Rombouts[2], Jozef Vleugels[1]

[1] *Department of Materials Engineering, KU Leuven, Kasteelpark Arenberg 44, B-3001 Heverlee, Belgium*
[2] *Coating and Shaping Technologies group, Flemish Institute for Technological Research - VITO, Boeretang 200, B-2400 Mol, Belgium*

samanwitha.kolli@kuleuven.be

Abstract
Additive manufacturing (AM) has recently emerged as a promising technology for producing copper (Cu) components with high conductivity for functional applications like electrical machines and heat exchangers. However, direct AM methods such as laser powder-bed fusion (LPBF) face limitations due to the intrinsic properties of pure copper such as high reflectivity. To overcome this, material extrusion additive manufacturing (MEX or MEAM) technology, specifically paste-based 3D micro-extrusion, shows great potential in processing pure copper. This indirect process involves layer-by-layer deposition of highly powder-loaded feedstock paste, followed by debinding and pressureless sintering. The limited research conducted so far on the manufacturing of pure copper using this technology has mainly demonstrated its ability to fabricate simple geometries. The objective of this study is to explore the design freedom for 3D micro-extrusion of Cu paste and analyze the manufacturing constraints associated with shaping geometrically complex structures. The manufactured components with features including thin walls, pins, tubes, and overhangs were characterized in various aspects, including metrology and part integrity by visual inspection, computed tomography, and dimensional accuracy. This involves shrinkage evaluation comparing the intended initial design, as-printed, and final post-thermal treatment parts. The results of this study were utilized to establish design rules and manufacturing constraints, thereby providing new insights into the potential of 3D micro-extrusion for producing complex components.

Extrusion-based printing; Pure Copper, Manufacturing constraints; Metrology; Computed tomography

1. Introduction

In terms of geometrical design freedom, additive manufacturing (AM) is emerging extensively with huge attention from academia and industry and has demonstrated its superiority over conventional manufacturing routes. Nevertheless, it is important to note that not all intricate features can be produced by AM [1]. Similar to the challenges posed by each AM technology to process certain materials, they also have their unique challenges in manufacturing certain geometrical features [2–4]. Of the viable AM technologies, paste-based material extrusion additive manufacturing (MEAM, referred to as 3D micro-extrusion in this work, is one of the promising AM technologies that offers to process a wide range of materials and fabrication of intricate geometries with high precision, zero wastage, and minimal post-processing steps. However, extrusion-based printing has so far mainly been explored for the fabrication of lattice structures and simple geometries of various materials to comprehend the paste printability, achievable density, and insights into the possible generation of internal voids and printing defects with limited studies on complex geometrical printing [5–7]. The present study focuses on exploring the design freedom for 3D micro-extrusion of dense pure copper for applications demanding enhanced complexity in the geometry for improved performance such as thermal management devices (heat exchangers and heat sinks). Pure copper is one of the essential materials for such applications for its high electrical and thermal conductivity. However, it poses challenges to laser powder bed fusion, the most commonly employed AM technology, due to its high reflectivity. This makes it more suitable for indirect AM such as extrusion-based printing. In this regard, extrusion-based printing, especially with paste as feedstock material, enables efficient processing of pure copper. This work presents an insight into the shaping/printing of dense pure copper parts comprising complex geometrical features using 3D micro-extrusion while addressing the associated criticalities and manufacturing constraints.

2. Experimental details

3D micro-extrusion involves feedstock paste preparation, printing, and drying followed by thermal treatment. The feedstock pastes were prepared by mixing 99.95% pure gas-atomized copper (d_{50} of 15 µm, Safina), a binder solution consisting of hydroxypropyl cellulose (HPC) in 1-propanol, and other additives in a planetary centrifugal mixer (Hauschild SpeedMixer DAC 1100). Mixing of the paste at atmospheric pressure was followed by a degassing step (mixing in vacuum) that enables the removal of air bubbles resulting in a dense paste. A high-precision 3D micro-extruder, 3Dn-450HP n-Scrypt, was employed for the shaping of the parts. The 3D printer works with a needle-type extrusion system with a smart pump, valve body, and valve rod. Complex geometry printing involves the adaptation of the printing parameters for individual intricate features. The green parts are set to dry for 4 days at room temperature before thermal treatment, involving debinding and sintering in a horizontal tube furnace in a 50/50 He/H_2 atmosphere. The parts were first subjected to debinding with a slow heating rate of 0.5 °C/min and a dwell time of 5 h at 550 °C followed by sintering at a heating rate of 5 °C/min and dwell time of 5 h at 1050 °C. The parts were characterized for dimensional accuracy through shrinkage measurements, before and after the thermal treatment, using microscopy and computed tomography. Detailed information on the feedstock paste and process optimization for 3D micro-extrusion of dense copper parts as well as their mechanical and physical properties are reported elsewhere [8].

3. Results and Discussion

3.1. Feedstock paste preparation

The characteristics of the feedstock paste and the initial raw material employed, i.e., the starting powder and type of binder, largely influence the flow and printability of the paste. The starting powder characteristics such as particle size and morphology determine the nozzle diameter which is essential for shaping parts with intricate geometries. It is recommended that the nozzle diameter is at least 10 times the maximum particle size for a starting powder with spherical morphology to prevent nozzle clogging and ensure smooth flow of the paste. Scanning electron micrograph of the pure copper reveal a distributed powder particle size with spherical morphology and fine satellites bonded to the coarser particles (Figure 1). On the other hand, the type of binder used for the feedstock paste preparation determines the rheological behaviour of the paste which is essential for extrusion-based printing. An ideal paste should exhibit a shear thinning behaviour, i.e. decreasing viscosity with an increasing shear rate, that ensures flow through the nozzle and stability of the fiber once deposited. This behaviour is imparted to the paste through the binder. The HPC binder used in the present work met the criteria making the feedstock pastes suitable for extrusion-based printing.

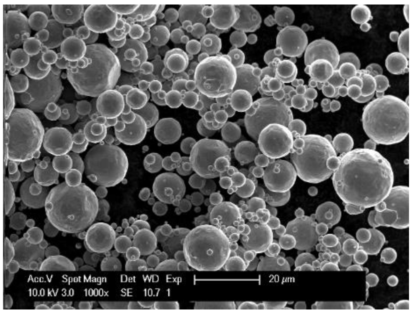

Figure 1. Scanning electron microscopy image showing the spherical morphology of the pure copper starting powder

3.2. Printing, thermal treatment and characterization

3D micro-extrusion of the highly viscous Cu paste was performed through a fine nozzle at room temperature (Figure 2a). The extruded filaments are deposited onto the printing substrate layer by layer adapting to the CAD design. The printing process requires the optimization of various parameters such as nozzle diameter, extrusion air pressure, inter-fiber distance, layer height or thickness, and printing strategy or fiber orientation. They significantly influence the final part density, and ultimate performance in terms of physical and mechanical properties [8]. These parameters also largely influence the geometrical precision and accuracy of the parts, especially in shaping intricate geometries. Since the global objective of the present work focuses on dense printing, the printing parameters were first optimized to achieve dense green parts and near fully dense sintered parts. Printing with the optimized set of printing parameters with a 400 µm nozzle followed by sintering (as discussed in Section 2) enabled the manufacturing of simple geometries with relative density in the range of 96-99% TD with an average isotropic shrinkage of 10-12%. Figure 2b shows the microstructure of a part with 97.23 ± 0.23% sintered density showing distributed closed residual porosity which is not associated with the printing process but a characteristic microstructural feature of a sintered part processed by the powder metallurgical route. Furthermore, to demonstrate the fabricability of complex-shaped dense copper components by 3D micro-extrusion, the design freedom offered by the technology was explored. In contrast to the printing of simple geometries, complex geometries demand consideration of various parameters to ensure not only the final part density but also precision in structure and dimensions. However, the set of these influential parameters significantly varies for each type of complex feature which will be discussed. The complex geometrical features relevant to heat exchangers and/or heat sinks such as thin walls, internal channels, and hollow pins were chosen for the investigation. The following subsections present the printability, stability, and metrology through dimensional accuracy along with the criticalities involved in printing such features thereby revealing the manufacturing constraints of the technology.

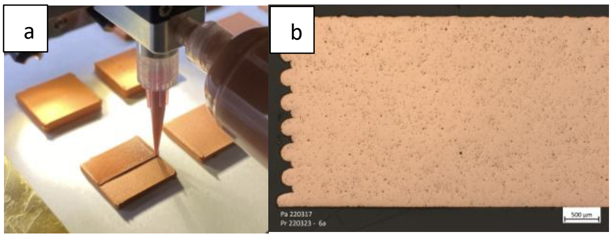

Figure 2. (a) Printing of viscous copper paste by 3D micro-extrusion, (b) Optical micrograph of the part, with a sintered relative density of 97.23%, printed with a 400 um nozzle

3.2.1 Walls

Walls of increasing height: Single-track walls (one fiber thick) of increasing height were built using 3D micro-extrusion. The maximum height of a single-track wall that can withstand the weight from the overlying layers, both during printing and thermal treatment, when printed using a particular nozzle size was assessed. Figure 3a, b, and c show the CAD, as-printed part with single-track walls with heights of 5, 7.5, 10, 12.5, and 15 mm printed with a 400 µm ceramic nozzle, and the sintered part, respectively. This demonstrated the printability of single-track walls to a height of 15 mm without any buckling or collapsing. Printing walls of different heights in a single part led to a changing wall thickness along their height with respect to the intended CAD design, as shown in Figure 3d presenting the thickness of all the walls in the center along their height as measured using a vernier calliper on a sintered part. The thickness of the upper end of the walls increased with increasing wall height, which could be attributed to the difference in drying time between the layers. When printing till the height of the shortest 5 mm wall, the drying time is the same for all the walls i.e. drying time for walls is equal to the time taken to deposit fibers on the other four walls. However, once the 5 mm wall is printed, the drying time between layers for the next four walls decreases to the time equal to the fiber deposition time on the rest of the three walls which resulted in a ~4 - 5 % increase in thickness. This continues till the printing of only the last and tallest 15 mm wall during which the drying time reduces to the time taken to deposit only one layer. For the 15 mm wall, the thickness of the last 2.5 mm (from the top) significantly increased by ~57% compared to the lower 5 mm wall (what could also be observed in Figure 5). This is because as the drying time decreases, the previously deposited fiber layer might slightly sag on the deposition of the subsequent layer, thereby resulting in a relatively thicker section of the wall. The overall shrinkage in thickness was observed to be 17.5% for the 5 mm wall.

Single-track 10 mm walls: Figure 4a, b, and d show the CAD, as printed, and sintered part with single track walls of 10 mm height printed using a 200 µm nozzle. The walls were printed and sintered at 950 °C for 3h without any noticeable deformation like bending or collapse as depicted in the top view (Figure 4c and e). The shrinkage in wall thickness was measured to be 20 ± 1%. In conclusion, it is feasible to employ 3D micro-extrusion with viscous Cu paste to produce single-track walls. However, printing of walls requires careful consideration of critical factors, including rheology of the paste and drying time between layers, as they directly impact the structural stability. Therefore, important printing parameters for wall fabrication include the nozzle diameter to achieve the desired thickness and printing speed to ensure enough drying time and maintain part integrity.

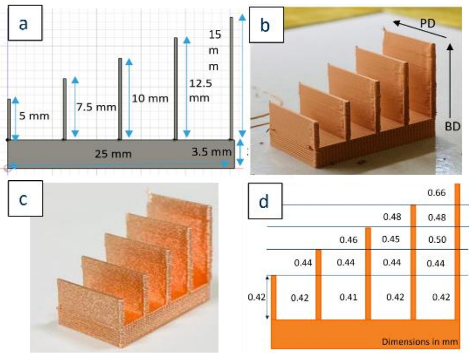

Figure 3. Part with walls of varying height printed using a 400 µm nozzle. (a) CAD, (b) as-printed, (c) sintered, and (d) schematic of the part after sintering showing varying dimensions along the height of the walls due to differences in drying time

The open and closed positions of the valve rod: They also affect the dimensional accuracy and final quality of the part. An improper choice of positions may lead to excess deposition of paste at the start of the wall (Figure 5, also seen in Figure 4b and d) and/or varied thickness along the width of the wall as it might take a few µm to mm before reaching the steady thickness. A change of around 5% in the wall thickness was observed along the width between the start and stop for the part shown in Figure 4. This could be improved by printing with alternative start positions for each layer which could compensate for the varying thickness.

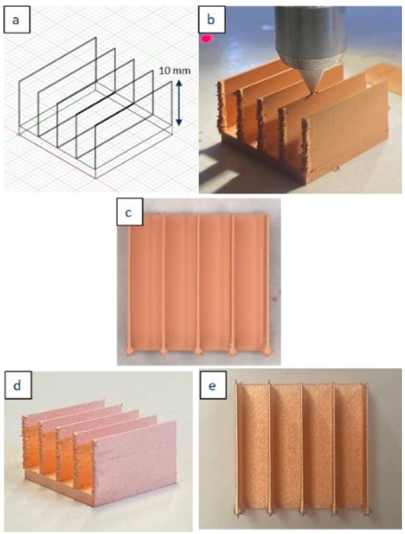

Figure 4. Part with walls of 10 mm height printed using a 200 µm nozzle. (a) CAD, (b,c) printed part, (d,e) sintered part

3.2.2 Internal channels

The printability of the finest internal channel was investigated. A cuboid with vertical internal channels of (intended) diameters 7, 5, 3, 1, and 0.5 mm was designed to print using a 250 µm nozzle. As shown in Figure 2b, the roughness of the part edges is determined by the printing strategy (unidirectional hexagonal

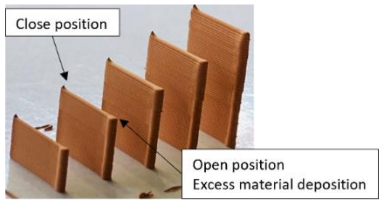

Figure 5. Walls printed using a 400 um nozzle depicting the excessive deposition of the paste at the start due to inappropriate open and close positions of valve rod in the nozzle

with decreased scan spacing and layer height**Error! Reference source not found.**) during printing, which can be a challenge for complex features like small internal channels, leading to significant deviations between layers. To address this issue, it is recommended to use a contour printing approach that ensures high precision. In reference to the g-code of the print with contour, the CAD file was adapted accordingly by increasing the feature dimension with respect to the nozzle diameter as illustrated in the schematic in Figure 6a. Figure 6b and c show the CAD with adapted dimensions and the as-printed part. Visual observation during printing indicated the feasibility of printing an internal channel as small as 0.5 mm (intended diameter) using a nozzle of 250 µm diameter, without any closure of the finest channel. Figure 6d shows the thermally treated part sintered to a relative density of 95.54% without visual deformation. A comprehensive CT analysis provided complete visualization of the part's structure as depicted in Figure 7, including an overview (Figure 7a), an image through the 7 mm channel (Figure 7b) and an image through the finest channel which shows that the channel remained open consistently throughout the thickness of the part (Figure 7c). Table 1 summarises the dimensional accuracy evaluation of the channel diameter with respect to the intended diameter for as-printed condition and as-printed for sintered, using stereomicroscopy data. The deviation between as-printed and intended diameter was highest for the finest channel. This could be attributed to two printing parameters: printing speed and the mass flow rate. The printing speed and the extrusion air pressure and therefore the mass flow rate remain the same throughout printing irrespective of the feature dimension. However, due to the continuous change in the direction while printing a circular dimension, i.e. the contour of the internal channel, the actual printing speed could be lower than the programmed one. The continuous change, maintaining the same mass flow rate, results in a thicker fiber with decreasing feature diameter. The overall sintering shrinkage decreased with decreasing channel diameter.

CT analysis also revealed the presence of porosity associated with printing, explaining the relatively low density of the part, as shown in Figure 7. Three types of voids/printing defects were observed in this part. First, voids at the junction of contours and the infill, both the outer contour and the internal channel contour, highlighted in green in Figure 7b. This is mainly attributed to the printing strategy (unidirectional hexagonal) that results in layers of two different lengths leading to this kind of defect. These types of voids could be avoided by employing an alternate printing strategy such as cross-printing. Second, voids within the infill (highlighted in red in Figure 7a). For complex geometries, printing as defined by the design is divided into sections within each layer leading to a discontinuity of the infill. A combination of this type of infill with the choice of fixed scan spacing could result in a mismatch between the number of fibers and the area of infill, causing defects. The third type of voids (highlighted in yellow in Figure 7b) are the periodic interfiber voids generated as a result of underfill due to insufficient mass flow rate or inappropriate choice of printing

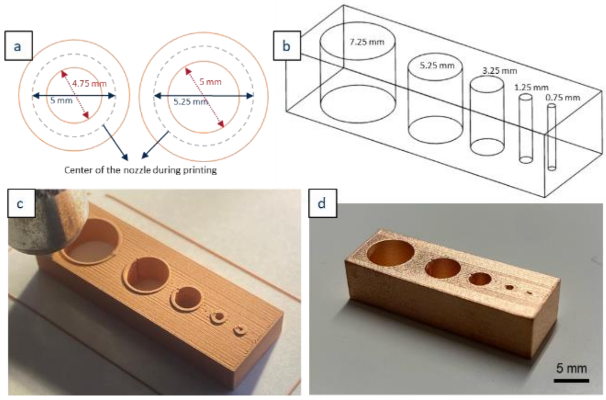

Figure 6. (a) Schematic showing the prerequisite adaptation of the CAD dimensions with respect to the nozzle diameter when printing the contour, (a) CAD, (b) as-printed, and (c) sintered part with vertical internal channels printed using a 250 µm nozzle

Table 1. Diameter dimensional accuracy evaluation of the part with vertical internal channels (Deviation of intended and as-printed)

CAD (mm)	7.25	5.25	3.25	1.25	0.75
Intended	7	5	3	1	0.5
As-printed	-1%	-2%	-2%(3.06)	-2%	9% (0.45)
Sintered	11%	10%	9%	8%	6%

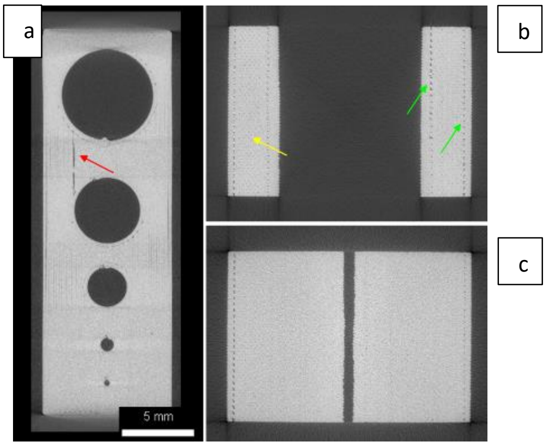

Figure 7. CT images of the part with internal channels post thermal treatment showing different types of porosity. (a) overview of the part showing voids within the infill (red), (b) image through a 7 mm channel showing interfiber voids (yellow) and voids between infill and contour (green), (c) image through the finest 0.5 mm channel

parameters such as overlap and layer height. The parameters optimized for a 400 µm nozzle were extrapolated and used for the printing of the part using a 250 µm nozzle. However, the interfiber voids present in the part indicate that the printing parameters were not transferrable.

3.2.3 Hollow pins

Similar to the vertical internal channels, hollow pins were printed to investigate the finest hollow pin that could be realized by 3D micro-extrusion. Hollow pin structures of 7, 5, 3, 1, and 0.5 mm (intended) inner diameters were designed to print using a 250 µm nozzle. Unlike the part with internal channels which was printed with a contour approach to improve the precision, it is the only approach that could be followed in this case as the cylindrical walls of the pins are achieved by the contour layers to realize a thin single fiber wall without infill. Therefore, the dimensions of the features were adapted accordingly with respect to the nozzle diameter. Figure 8a, b, and c show the CAD, as-printed part, and part sintered at 1050 °C, respectively. The finest hollow pin that was printable without collapse or distortion was that with a CAD of 0.75 mm inner diameter

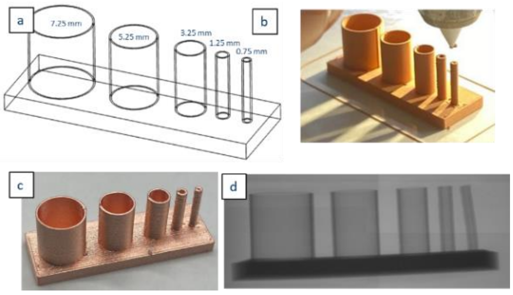

Figure 8. (a) CAD, (b) printed, and (c) sintered part with hollow pins printed using a 250 µm nozzle along with a (d) CT scan

intending to produce a 0.5 mm pin. After sintering, the CT scan in Figure 8d revealed that the pins retained their original shape, remaining intact and straight without signs of deformation (the distortion of the finest pin was due to mishandling during CT analysis). It also shows that the finest pin with an as-printed diameter of 0.33 mm and a sintered diameter of 0.32 mm remained open through the thickness.

4. Conclusions

Design freedom offered by 3D micro-extrusion of highly viscous pure copper paste was explored to establish design rules and put forth the manufacturing constraints. Copper pastes with suitable rheology were used for the shaping of parts with intricate geometries. Features relevant to heat exchangers and heat sinks were printed and sintered including single-track walls, vertical internal channels, and hollow pins. 3D micro-extrusion enabled the fabrication of all considered features with minimal to no visual deformation or shape distortion during printing and sintering. A part with walls of 10 mm height and a final thickness of 280 µm was successfully produced using a 200 µm nozzle. The walls neither collapsed nor showed any buckling during the entire processing route. Using a 250 µm nozzle, the technology allowed manufacturing parts with a finest vertical internal channel of 0.43 mm and hollow pin of 0.32 mm diameter. The geometrical assessment using computed tomography showed that the parts' shapes were preserved without any noticeable deformation with the finest features remaining open throughout the thickness. This indicated the printing and thermal treatment cycle were effective in producing high-quality parts. However, there are criticalities and concerns which are to be addressed such as defects generated when printing with a contour, excessive paste extrusion at the start, and the printing parameters that need optimization to eliminate interfiber voids.

References

[1] Meisel N and Williams C 2015 *Journal of Mechanical Design, Transactions of the ASME* **137** no. 11 1–9

[2] Thompson M K et al. 2016 *CIRP Annals Manufacturing Technology* **65** no. 2 737–760

[3] Allison J, Sharpe C, and Seepersad C C 2018 *Additive Manufacturing* **25** 239–251

[4] Patterson A E, Chadha C, and Jasiuk I M 2021 *Journal of Manufacturing and Materials Processing* **5** no. 2

[5] Lieberwirth C, Harder A, and Seitz, H 2017 *Journal of Mechanics Engineering and Automation* **7** no. 2

[6] Rane K and Strano M 2019 *Additive Manufacturing* **7** no. 2 155–173

[7] Sun X, Mazur M, and Cheng C T 2023 *Additive Manufacturing* **67** 103463

[8] Kolli S, Beretta M, Selema A, Sergeant P, Kestens L A, Rombouts M, and Vleugels J 2023 *Additive Manufacturing* **73** 103670